Time-Resolved Impulsive Stimulated Raman Scattering from Excited-State Polyatomic Molecules in Solution

Satoru Fujiyoshi,[†,‡] Satoshi Takeuchi,[‡] and Tahei Tahara*[,‡]

Department of Structural Molecular Science, The Graduate University for Advanced Studies, Myodaiji, Okazaki 444-8585, Japan, and Molecular Spectroscopy Laboratory, The Institute of Physical and Chemical Research (RIKEN), 2-1 Hirosawa, Wako 351-0198, Japan

Received: September 27, 2002; In Final Form: November 13, 2002

Time-domain Raman measurement of the excited state of a polyatomic molecule was demonstrated for the first time. Time-resolved impulsive stimulated Raman scattering (TR-ISRS) measurements were carried out for *trans*-stilbene in solution, and resonantly enhanced signals due to the S_1 state were observed under the resonance condition with the $S_n \leftarrow S_1$ absorption. The observed signal consisted of a spike-like feature around the time origin, an oscillatory component with a period of ∼0.12 ps, and a slowly decaying traditional transient-grating (TG) signal. A Fourier transform analysis clarified that the oscillatory ISRS component was attributed to an in-plane bending vibration of S_1 *trans*-stilbene (ν_{24}, 285 cm^{-1}). The origin of the TG signals was examined by three-pulse absorption measurements, and it was concluded that the transient grating was created reflecting two relaxation processes following the $S_n \leftarrow S_1$ excitation: the vibrational cooling process of S_1 *trans*-stilbene and the loss of the S_1 population. The present study demonstrated that time-resolved time-domain Raman spectroscopy can provide spectral information about low-frequency tetrahertz motions of the excited-state, which cannot be accessed by ordinary time-resolved frequency-domain Raman spectroscopy.

1. Introduction

Time-resolved Raman spectroscopy is a very powerful tool for the study of photochemistry and photophysics, and it affords unique information about the molecular structure, dynamics and properties of short-lived transient species.[1−9] In the experiments of time-resolved Raman spectroscopy, the pump pulse is first irradiated to generate transient species (or start photochemical reactions), and then the probe pulse is introduced after a certain delay time to monitor Raman scattering (Figure 1a). To examine the temporal change of the sample, a set of Raman spectra are measured by changing the delay time between the pump and probe pulses. The probe wavelength is usually tuned to the electronic absorption of the transient species of interest, to take advantage of the selective intensity enhancement due to the resonance effect. This time-resolved Raman spectroscopy is widely utilized, especially for the measurement of the vibrational spectra in the fingerprint region. However, observation of the low-frequency vibration of the transient species is often very difficult because of the disturbance of strong Rayleigh scattering. Observation of the low-frequency vibration in the terahertz region attracts much interest because unique vibrations such as large amplitude motions appear.

Recently, thanks to the development of ultrashort-pulse lasers, Raman-active low-frequency vibrations can be observed not only in the frequency domain but also in the time-domain by using femtosecond spectroscopy. Transient-grating type impulsive stimulated Raman scattering (ISRS) spectroscopy[10−16] and Raman-induced Kerr effect spectroscopy (RIKES)[17−20] have been widely utilized for time-domain Raman measurements. For example, Ruhman et al. reported that the femtosecond ISRS signal from CS_2 liquid exhibits overdamped intermolecular motion,[11] which demonstrated that the time-domain method with a sufficient time-resolution clearly detects Raman-active motion of the liquid sample. Optical heterodyne detected (OHD-) ISRS and OHD-RIKES are highly capable in the time-domain Raman measurements.[14,15,21−24] It was shown that the Fourier transform analysis of the observed OHD signal can provide spectra equivalent to the Raman spectra in the low-frequency region.

In principle, the information obtained by time-domain Raman spectroscopy is equivalent to that given by the traditional

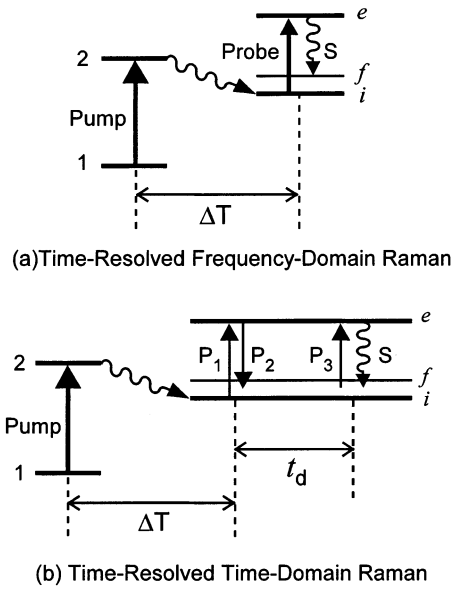

Figure 1. Experimental schemes of two types of time-resolved Raman spectroscopy. (a) Time-resolved frequency-domain Raman spectroscopy. (b) Time-resolved time-domain Raman spectroscopy

* Author to whom correspondence should be addressed. Fax: +81-48-467-4539. E-mail: tahei@postman.riken.go.jp.

† Department of Structural Molecular Science, The Graduate University for Advanced Studies.

‡ Molecular Spectroscopy Laboratory, The Institute of Physical and Chemical Research (RIKEN).

10.1021/jp0270856 CCC: $25.00
Published on Web 01/07/2003

frequency-domain Raman spectroscopy. However, time-domain spectroscopy is advantageous over the frequency-domain Raman spectroscopy for the measurements of low-frequency vibrations, because Rayleigh scattering is readily separated. For example, Castner, et al. obtained the Raman spectrum of water in a wide frequency region from 0 to 1200 cm^{-1}, by combining the data taken in the time-domain measurement (for the low-frequency region) and the frequency-domain measurement (for the high-frequency region).[23] Therefore, if we apply time-domain Raman spectroscopy for the transient species that are generated by the laser irradiation, it is expected that we can observe low-frequency transient Raman spectra that are difficult to be measured by ordinary time-resolved (frequency-domain) Raman spectroscopy. Banin and Ruhman demonstrated a time-domain measurement for low-frequency vibrations of the diiodide ion that is created from the triiodide ion by photodissociation.[25] However, time-domain Raman measurements for transient species are very scarce and only a few studies for small photoproducts have been reported.[25−28]

In this paper, we report the first application of time-domain Raman spectroscopy to the excited-state polyatomic molecule in solution. We carried out the transient-grating type ISRS measurement for the S_1 state of *trans*-stilbene and observed the low-frequency vibration of the excited state in the time-domain. The aim of the present study is two-fold: (1) examination of the potential of "time-resolved time-domain Raman spectroscopy" for the study of the excited-state polyatomic molecules, and (2) clarification of the origins of the signals that are observed in this type of new time-resolved Raman spectroscopy.

2. Experimental Section

2.1. Experimental Principle. Figure 1b shows a schematic diagram of the experimental principle of time-resolved time-domain Raman spectroscopy. In this experiment, the pump pulse is irradiated on the sample to electronically excite molecules ($2 \leftarrow 1$). After a certain delay time (ΔT), the time-domain Raman measurement is carried out as "the probe process", for which the transient-grating type ISRS measurement is adopted in the present study. The two femtosecond pulses, the first and second probe pulses (P_1 and P_2), are simultaneously introduced to the sample with a crossed angle, creating a spatially periodic distribution of refractive index (Δn) and absorbance (Δk) variations (transient-grating). The amplitude of the generated transient grating is monitored by the diffraction of the third femtosecond probe pulse (P_3) that is introduced after a delay time (t_d). If the duration of the probe pulse is sufficiently shorter than the period of the Raman-active vibrations, the P_1 and P_2 pulses create vibrational coherence in the excited-state that is generated by pump pulses. This coherence gives rise to oscillatory modulations in the transient-grating amplitude, and hence the intensity of the diffraction of the P_3 pulses shows oscillations associated with the molecular vibrations. The wavelength of the three probe pulses is tuned to the absorption of the excited-state molecules to take advantage of resonance intensity enhancement. The delay time ΔT between the pump and the probe processes corresponds to the delay time in ordinary time-resolved frequency-domain Raman spectroscopy, whereas the delay time t_d is scanned for the time-domain measurement of Raman-active vibrations.

2.2. Experimental Setup. Figure 2 shows the apparatus that was constructed for the present study. The light source was a Ti:sapphire regenerative amplifier system (Clark-MXR, CPA-1000) seeded by a mode-locked Ti:sapphire laser (Coherent, MIRA-900F). The amplified pulse having a 100-fs duration (800 nm, 1 mJ, 1 kHz) was divided into two parts. One portion (0.3 mJ) was converted to the third harmonic (267 nm) by using LiB_3O_5 and β-BaB_2O_4 crystals. The generated ultraviolet subpicosecond pulse (550 fs) was used as the pump pulse to create excited-state molecules. It was focused into a 300 μm-thick film-like jet stream of the sample solution. At the sample position, the energy of the pump pulse was $\sim$7 μJ, and the spot diameter was $\sim$300 μm. The other portion of the amplified pulse (0.7 mJ) was converted to a near-infrared pulse (1220 nm, 70 μJ) in an optical parametric amplifier (Quantronix, TOPAS). This near-infrared pulse was subsequently frequency-doubled in a 0.5-mm-thick β-BaB_2O_4 crystal to generate a visible pulse (610 nm). It was used for the probe process, i.e., the transient-grating measurements. The visible pulse was as short as 40 fs in duration after the dispersion compensation using a prism pair. This visible femtosecond pulse was divided into two, and each pulse was diffracted into two ($\pm$1 orders) by a phase mask. One of the created four pulses was blocked and the other three pulses (P_1, P_2, and P_3) were focused onto the photoexcited portion of the sample with a standard BOXCARS geometry. At the sample position, the energies of the P_1, P_2, and P_3 pulses were 0.2 μJ, 0.2 μJ, and 0.1 μJ, respectively, and their spot diameter was $\sim$200 μm. Polarizations of the three visible probe pulses were set parallel with one another. The intensity of the signal light diffracted to the phase-matched direction was detected by a photodiode (S1337-1010BQ, Hamamatsu), and its output was processed on a shot-to-shot basis by using a boxcar integrator (Stanford Research Systems). The polarization of the ultraviolet pump pulse was set at the magic angle (54.7°) with respect to that of the visible probe pulse.

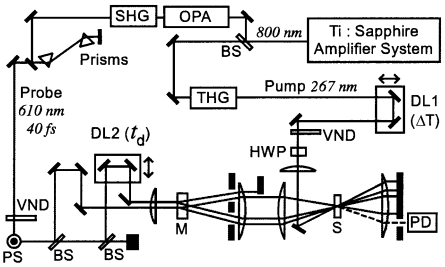

Figure 2. Apparatus used for TR-ISRS measurements: DL1 and DL2, optical delay lines; BS, beam splitter; OPA, optical parametric amplifier; SHG, second harmonic generation; THG, third harmonic generation; VND, variable neutral density filter; PS, periscope; M, phase mask; HWP, half-wave plate; PD, photodiode; S, sample solution.

Transient absorption measurements with a subpicosecond time-resolution were carried out with use of the setup reported previously.[29] The setup is based on the same femtosecond Ti:sapphire regenerative amplifier system, but it is operated at 100 Hz. The third harmonic of the amplified pulse is utilized as the pump, while a white-light continuum generated in D_2O is used for monitoring the time-resolved absorption. Spectra of the probe and reference lights are simultaneously measured by a CCD detector that is synchronized with the laser pulse. Measurements at the magic angle (54.7°) are achieved by rotating the pump polarization with respect to the probe polarization. Three-pulse absorption measurements were also performed using this setup, by introducing the second harmonic of the OPA output.

trans-Stilbene was purchased from Tokyo Kasei. It was recrystallized twice from cyclohexane, and was subsequently dried in vacuo before use. Ethanol (Wako Pure Chemical, 99.5%), methanol (nakalai tesque, spectroscopic grade), heptane (Wako Pure Chemical), and decane (Aldrich, 99%+ anhydrous) were used without further purification. The con-

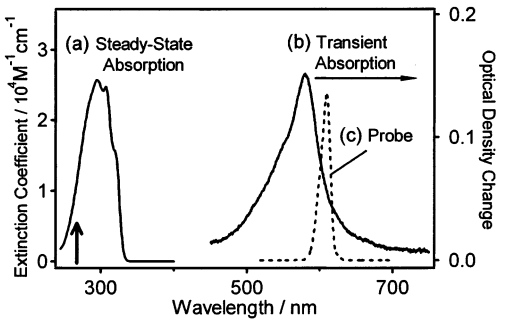

Figure 3. (a) Steady-state absorption spectrum of *trans*-stilbene in ethanol. (b) Transient absorption spectrum of *trans*-stilbene in ethanol (5.5×10^{-3} mol dm^{-3}) measured at 20 ps after photoexcitation at 267 nm (indicated by an arrow). (c) Spectrum of the probe pulse used in the TR-ISRS measurements.

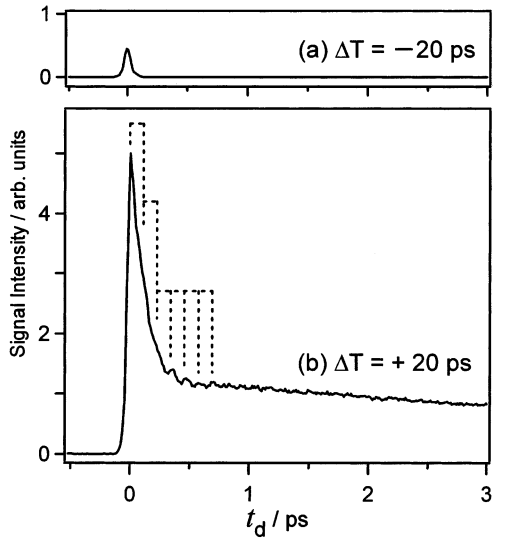

Figure 4. TR-ISRS signals of *trans*-stilbene in ethanol (5.5×10^{-3} mol dm^{-3}) measured at $\Delta T = -20$ ps (a) and $\Delta T = +20$ ps (b).

centration of the sample solution was 5.5×10^{-3} mol dm^{-3} for all the measurements.

3. Results and Discussion

3.1. Signal Observed in TR-ISRS Measurements. In this study, we carried out time-resolved impulsive stimulated Raman scattering (TR-ISRS) measurements for *trans*-stilbene. Figure 3a shows the absorption spectrum of *trans*-stilbene in ethanol. The strong absorption band in the ultraviolet region is assigned to the S_1 ($\pi\pi^*$) $\leftarrow$ S_0 transition. Photoexcitation of *trans*-stilbene through this S_1 ($\pi\pi^*$) $\leftarrow$ S_0 transition gives rise to a strong transient absorption in the visible region. Figure 3b depicts the transient absorption measured at 20 ps after photoexcitation at 267 nm. The transient spectrum shows a broad intense band around 580 nm. This transient band is assigned to the absorption of the planar S_1 state of *trans*-stilbene.[30] In ethanol, this S_1 absorption decayed with a time-constant of 62 ps, which corresponds to the time constant of the isomerization in the S_1 state.[31,32]

We photoexcited *trans*-stilbene in ethanol with 267-nm pump pulses, and carried out TR-ISRS measurements using probe pulses at 610 nm. Figure 4 depicts the signals obtained from the TR-ISRS measurements. In the measurement carried out before photoexcitation ($\Delta T = -20$ ps), only a spike-like response was observed around the time origin of the ISRS measurement ($t_d = 0$ ps), as shown in Figure 4a. This signal is attributed to the nonresonant electronic response of the solvent molecule. The signal due to S_0 *trans*-stilbene could not be recognized with this signal-to-noise ratio, because the concentration of *trans*-stilbene was low and its absorption is far from the probe wavelength (nonresonant condition). The observed nonresonant electronic response of the solvent was well fitted by a Gaussian function having a full-width at half-maximum (fwhm) of 66 fs. It corresponds to the instrumental response of the present ISRS measurements because nonresonant electronic response is instantaneous. On the other hand, in the ISRS measurement performed at the delay time of 20 ps ($\Delta T = 20$ ps), a very strong signal having complicated features was observed, as shown in Figure 4b. The peak intensity of the signal becomes 10 times larger than the solvent electronic response that was measured before photoexcitation. This drastic increase of the signal intensity is apparently related to the generation of S_1 *trans*-stilbene. Since the probe wavelength of the ISRS measurement (610 nm) is in rigorous resonance with the $S_n \leftarrow S_1$ transition of *trans*-stilbene, the signal associated with S_1 *trans*-stilbene is expected to gain high-intensity enhancement. Therefore, it is safely concluded that the strong signal observed at $\Delta T = 20$ ps is solely attributable to S_1 *trans*-stilbene, although the concentration of the stilbene molecule was as low as 5.5×10^{-3} mol dm^{-3}.

The signal observed at $\Delta T = 20$ ps after photoexcitation is rather complex. First, it exhibits a spike-like ultrafast feature around the time-origin of t_d. Second, an oscillatory feature is observed in the time range up to 1 ps. Obviously, this feature is ISRS. Third, an offset-like signal is seen in the positive t_d time, which slowly decays in the time range of $\sim$100 ps. This slow signal component is attributed to the traditional transient-grating (TG) signal.

Concerning the first spike-like ultrafast feature, one of the origins is considered to be the resonant electronic response of S_1 *trans*-stilbene. In the third-order nonlinear Raman spectroscopy in the frequency domain such as CARS, it is known that the electronic resonance term of the solute molecule gives rise to the "white" background signal (the resonant background), when the probe wavelength matches the absorption of the molecule.[33−35] In the time-domain measurement, the corresponding electronic response is expected to appear as an "almost instantaneous" signal around the time-origin of t_d. Thus, it is highly likely that the resonant electronic response of S_1 *trans*-stilbene contributes to the first ultrafast feature. However, the ultrafast feature seems to contain another component, because it showed asymmetric shape in time (Figure 5a). This strongly indicates the coexistence of the component having a finite lifetime. In fact, a fitting analysis taking account of the instrumental response suggested that the ultrafast feature consists of two components, the instantaneous response (which is assignable to the resonant electronic response) and the response having a lifetime of $\sim$100 fs. We tentatively assigned this 100-fs component to the S_n population grating. Since the probe wavelength is resonant with the $S_n \leftarrow S_1$ transition, the first set of the probe pulses (P_1 and P_2) excites S_1 *trans*-stilbene to the S_n state and generates a transient grating arising from the difference in the population of the S_n and S_1 states. This S_n population grating should disappear with a time constant equivalent to the lifetime of the S_n state. The evaluated lifetime of the 100-fs component is a typical lifetime of the highly excited singlet (S_n) states,[36−38] which supports this assignment. Therefore, we concluded that the ultrafast feature around the t_d time origin arises from the resonant electronic response of the S_1 state as well as the S_n population grating of *trans*-stilbene.

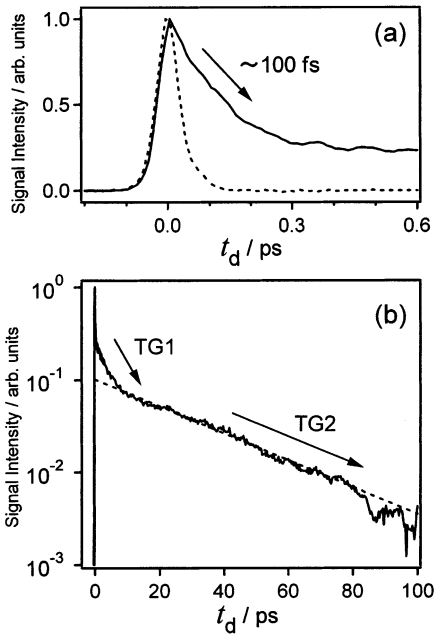

Figure 5. (a) TR-ISRS signals of *trans*-stilbene in ethanol measured at $\Delta T = -20$ ps (broken curve) and $\Delta T = +20$ ps (solid curve) for the early t_d time range. The signal intensities are normalized. (b) TR-ISRS signals of *trans*-stilbene in ethanol measured at $\Delta T = +20$ ps (solid curve) for a wide t_d time range (from −3 to 100 ps). The best single-exponential fit to the TG2 component is also shown with a broken line.

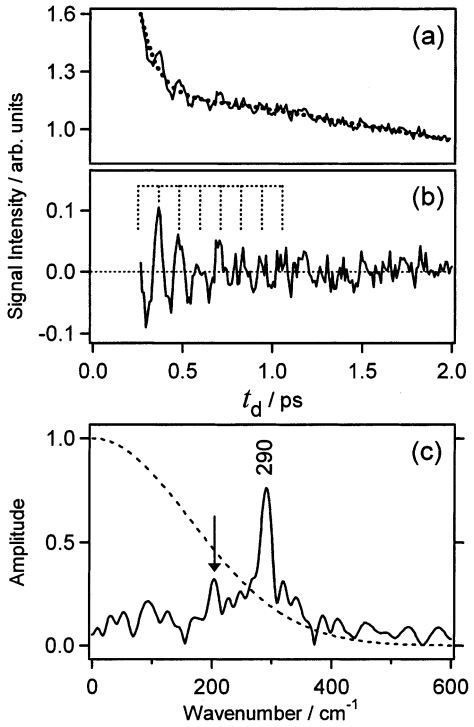

Figure 6. (a) Calculated ultrafast and TG components (dotted line) compared with the TR-ISRS signal. (b) Oscillatory component obtained by the subtraction procedure. (c) The amplitude spectrum obtained by the Fourier transform analysis of the oscillatory component (solid curve). The effective sensitivity curve of this time-domain measurement is shown with a broken curve (see text).

The second (ISRS) and the third (TG) features in the signal are separately discussed in detail in the following sections.

3.2. Impulsive Stimulated Raman Scattering from S_1 Stilbene. The oscillatory component observed in the time range of ~1 ps is no doubt ascribable to the ISRS signal. In addition, it is safely assigned to the ISRS of S_1 *trans*-stilbene, because the oscillatory signal was observed only in the TR-ISRS measurement performed after photoexcitation.

Before describing the analysis of this ISRS component, we argue that the observed ISRS signal was practically heterodyned, although the diffracted signal was directly detected in the present experiment (homodyne detection). As shown in Figure 4, the oscillatory component was observed on the slowly decaying TG component. Therefore, the intensity of the detected signal is expressed as

$$I_{obs} = |E_{osc}\, e^{i\theta} + E_{TG}\, e^{i\phi}|^2 = E_{osc}{}^2 + 2E_{osc}E_{TG}\cos(\theta - \phi) + E_{TG}{}^2 \quad (1)$$

for the t_d time region of 0.3−1 ps when the ultrafast feature has already vanished. Here, E_{osc} and E_{TG} are the amplitude of the electric field of the ISRS and TG components, respectively, whereas θ and ϕ are their phases with respect to the phase of the electric field of the third probe pulse (P_3). As this formula indicates, the two components, the oscillatory ISRS component and the TG component, can interfere with each other to give rise to the second term, unless these two components are completely out of phase ($\theta - \phi = \pm\pi/2$). It has been experimentally and theoretically proved that, under the resonance condition, the electric field of the time-domain Raman signal involves both in-phase and quadrature-phase parts with respect to the phase of the incident pulse.[22] It is also known that the traditional grating yields the in-phase and quadrature-phase parts in the diffracted signal.[39−41] Consequently, the ISRS and the TG components should have parts having a common phase, and they can significantly interfere. Since the amplitude of the ISRS component is much smaller than that of the TG component ($|E_{osc}| \ll |E_{TG}|$), the first term in eq 1 becomes negligibly small. Thus, if we neglect a small temporal change of the TG component in the relevant early time region (<1 ps), we can consider that the ISRS signal is heterodyned in a practical sense, and that the observed oscillatory ISRS component is linearized to the Raman-active nuclear response of S_1 *trans*-stilbene.

To analyze this heterodyned ISRS component, we extracted the oscillatory component from the observed signal. As depicted in Figure 6a, we fit the sum of the exponential functions to the ultrafast feature and the slow TG component,[42] and subtracted it from the obtained data. The extracted oscillatory component is depicted in Figure 6b. Since the subtraction in the early time region can have error due to very rapid temporal change of the ultrafast component, we only focused the time region after 0.26 ps and calculated Fourier transform of the extracted oscillatory component in the time region of 0.26−2 ps.[43] Figure 6c shows the amplitude spectrum of the obtained Fourier transform (the square root of the sum of squares of the real and imaginary parts), which is the frequency-domain representation of the observed Raman active vibrations. In this figure, we also plotted the "effective sensitivity" of the present time-domain measurement that was calculated from the observed instrumental response (broken line).[44] As this sensitivity curve indicates, the spectral information below 400 cm^{-1} can be obtained from the present measurement.

The Fourier transform of the ISRS component clearly exhibits a strong peak at ~290 cm^{-1}. This frequency agrees very well with the frequency of an in-plane bending vibration (ν_{24}, 285 cm^{-1}) of S_1 *trans*-stilbene that has been observed by frequency-domain Raman spectroscopy.[45,46] In fact, the Raman spectra of S_1 *trans*-stilbene has been measured for the frequency region

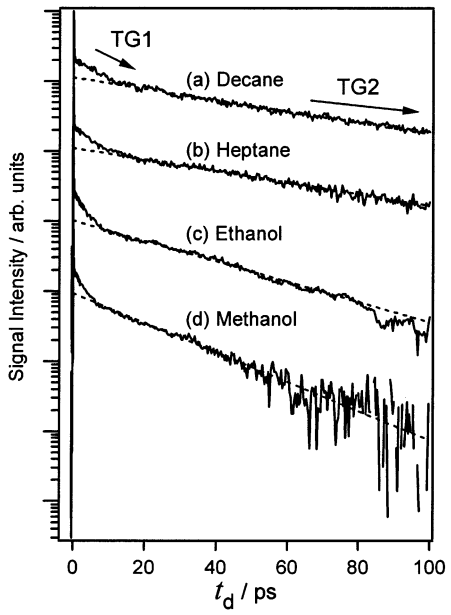

Figure 7. Logarithmic plot of the TG signals measured at $\Delta T = 20$ ps in decane (a), heptane (b), ethanol (c), and methanol (d). Each signal is vertically shifted by an order of the magnitude. The best single-exponential fits to the TG2 components are also shown with broken lines.

TABLE 1: Evaluated Lifetime of the TG2 Component and the S_1 Lifetime of *trans*-Stilbene in Four Solvents

solvent	TG2 lifetime[a]/ps	S_1 lifetime/ps
decane	100	137
heptane	96	106
ethanol	57	62
methanol	42	49

[a] Double of the apparent decay time.

above 200 cm^{-1}, and it has been reported that two Raman bands appear in the frequency region of 200−400 cm^{-1}: a strong band at 285 cm^{-1} (ν_{24}) and a very weak band at 200 cm^{-1} (ν_{25}). In the Fourier transform of the ISRS component, a small peak was also recognized at 200 cm^{-1} (marked by an arrow), which highly likely corresponds to the second weak S_1 Raman band assigned to the ν_{25} mode. The relative intensity of these two Raman-active S_1 vibrations observed in the time-domain measurement is very consistent with the frequency-domain Raman data.[45] This result clearly shows that TR-ISRS spectroscopy can afford information about the Raman-active low-frequency vibrations of excited-state polyatomic molecules in solution.

3.3. Slow Traditional Transient Grating Signal. The slowly decaying signal in the t_d time range up to ∼100 ps is ascribable to the traditional TG signal. Since this TG signal acts as the local oscillator to heterodyne the ISRS signal, the clarification of its origin is important for full understanding of the present TR-ISRS measurement. As shown in a logarithmic plot of the observed signal for a wide t_d time region (Figure 5b), the TG component is bimodal: it first decreases rapidly in the t_d range up to ∼10 ps, and then exhibits a single-exponential decay afterward. This suggests that the observed traditional TG signal has two different origins. For convenience, we refer to these two TG components as TG1 (∼10 ps) and TG2 (∼100 ps), hereafter. The precise evalutation of the lifetime of the TG1 component was difficult owing to the temporal coexistence of the two components (TG1 and TG2) in the homodyne-detected signal. The lifetime of TG2, however, was directly evaluated from the trace in the t_d region after 20 ps when the signal exhibits a single-exponential decay. By a fitting analysis taking account of the self-absorption effect,[47] the lifetime of TG2 was evaluated as 57 ps in ethanol. (The lifetime is double the apparent decay time in the case of homodyne detection.)

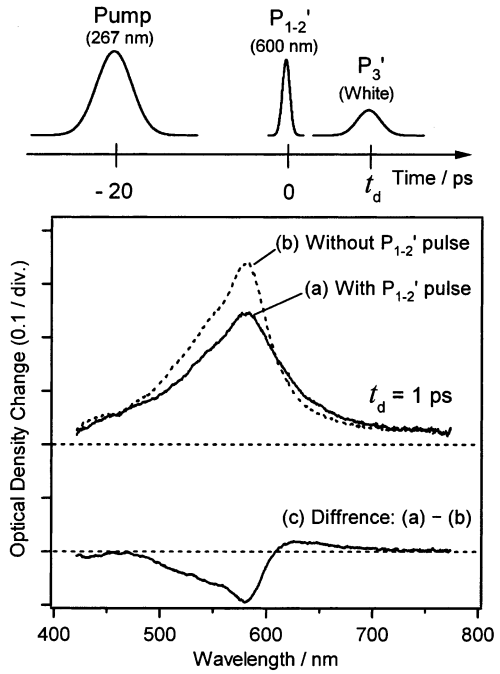

Figure 8. (a) $S_n \leftarrow S_1$ absorption of *trans*-stilbene in ethanol at the delay time $t_d = 1$ ps with the visible irradiation. (b) $S_n \leftarrow S_1$ transition of *trans*-stilbene in ethanol at the delay time $t_d = 1$ ps without the visible irradiation. (c) The difference spectrum: (a) − (b). Pulse sequence of the three-pulse transient absorption measurement is also shown at the top of the figure.

The lifetime of the TG2 component agrees very well with the lifetime of S_1 *trans*-stilbene in ethanol (62 ps). To confirm this agreement, we measured the TG signal in several solvents. Figure 7 shows the TG components measured at $\Delta T = 20$ ps in four solvents—decane, heptane, ethanol, and methanol. In all solvents, the TG signal showed a bimodal feature. Nevertheless, it exhibited a single-exponential decay in the t_d time region after 20 ps. The evaluated lifetime (double the apparent decay time) of the TG2 component was compared with the S_1 lifetime in Table 1. The two lifetimes showed very good agreement in all the solvents.

One may think that TG2 is attributable to the S_1 population grating, because its lifetime coincides with the S_1 lifetime. However, this is not the case, because the S_1 state is generated by the pump pulse, but not by the P_1 and P_2 pulses that create the transient grating. Actually, clarification of the origin of the TG signal needed an effort.

The appearance of the slowly decaying TG signal implies that a periodic modulation lasts in the sample for a time as long as 100 ps after the irradiation of the first two probe pulses (P_1 and P_2). In other words, some optical-property difference persists between the bright and dark parts of the interference pattern of the P_1 and P_2 pulses during the lifetime of S_1 *trans*-stilbene. To elucidate the origin of the TG components, we performed a three-pulse experiment that is sketched in Figure 8 (top). In this experiment, at 20 ps after the generation of the S_1 state by the pump pulse, a visible pulse at 600 nm (P_{1-2}') was introduced to the sample. This pulse is considered to induce a change that is equivalent to the change induced in the bright part of the interference of the P_1 and P_2 pulses. Then, a femtosecond white-

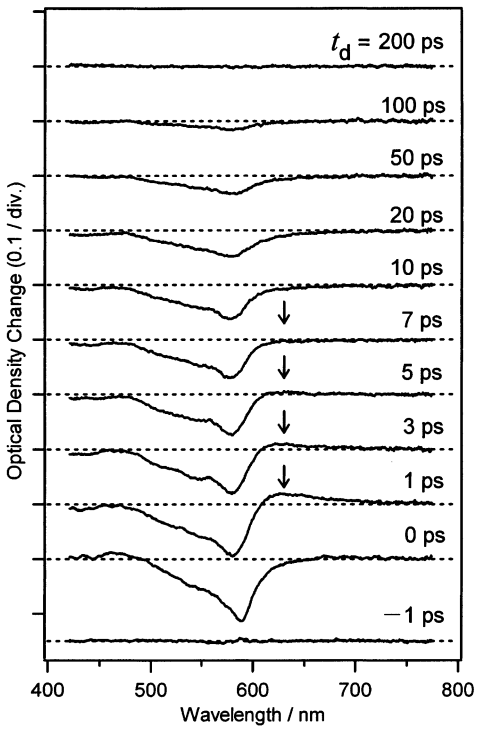

Figure 9. Three-pulse transient absorption spectra of *trans*-stilbene in ethanol (5.5×10^{-3} mol dm^{-3}) measured at various delay times from −1 to 200 ps.

continuum (P_3') pulse is irradiated to monitor the absorption of the sample after a time delay corresponding to t_d. As readily understood, this three-pulse experiment mimics the TR-ISRS measurement, and provides spectral information about the origin of the observed TG signal.

Figure 8a shows the absorption spectra obtained by the three-pulse experiment. The delay time between P_{1-2}' and P_3' was set at 1 ps, and their polarizations are parallel with each other and are set at the magic angle (54.7°) with respect to the polarization of the pump pulse. For comparison, the spectrum measured without P_{1-2}' irradiation is also shown in Figure 8b. (This corresponds to the spectrum of the dark part of the interference.) Basically, both spectra are transient absorption spectra of S_1 stilbene. However, the spectra observed with and without the P_{1-2}' pulse are significantly different: With irradiation of the P_{1-2}' pulses, (1) the S_1 absorption decreased its intensity, and (2) showed a band broadening. Figure 8c depicts the difference between the S_1 absorption spectra observed with and without P_{1-2}' excitation. This difference spectrum represents the difference in the optical properties between the bright and dark area of the interference between P_1 and P_2 pulses, which gives rise to the observed TG signal. To consider the relation of the observed spectral difference and the two TG components, we performed three-pulse experiments by changing t_d time. The observed temporal change of the difference spectrum is shown in Figure 9. As clearly shown, the S_1 absorption bleached with the irradiation of the P_{1-2}' pulse, and showed band broadening within 1 ps. (The band broadening is represented by the positive feature around 630 nm in the difference spectra, which is marked by arrows.) The S_1 band broadening disappeared within 10 ps, whereas the bleaching feature lasted in a time region as long as 100 ps. We made a fitting analysis using a biexponential function, and evaluated lifetimes of 6 and 64 ps for the band broadening and bleaching features, respectively. These time constants agree well with the temporal behaviors of the TG1 and TG2 components in the TR-ISRS measurement. Therefore, it is safely concluded that the physical origins of TG1 and TG2 are the same as the origin of the band broadening and bleaching of the S_1 transient absorption observed in the three-pulse experiment. We note that the lifetime of the bleaching of the S_1 absorption is naturally the same as that of the S_1 absorption, because the intensity difference vanishes when the S_1 absorption itself disappears.

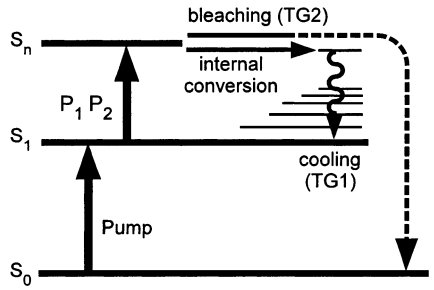

Figure 10. Schematic diagram of the relaxation process following the $S_n \leftarrow S_1$ excitation, which gives rise to the slowly decaying TG signal.

The spectral data obtained by the three-pulse experiments enabled us to assign the origin of the TG signals straightforwardly. Since the wavelength of the probe pulses matches the $S_n \leftarrow S_1$ absorption, the P_1 and P_2 pulses excite the S_1 state to the S_n state. A portion of the photoexcited S_n state returns to the S_1 state but the other does not. A significant amount of photoexcited S_n state is relaxed via different pathways, giving rise to net loss of the S_1 population. This causes bleaching of the S_1 absorption. This bleaching of the S_1 signal due to the intense probe irradiation is very often observed in the time-resolved frequency-domain Raman measurements.[48] Thus, the interference of the P_1 and P_2 pulses leads to a spatially periodic bleaching of the S_1 state, which acts as a transient grating. This "bleaching grating" is the origin of the TG2 component. The other portion of the photoexcited S_n state is relaxed to the S_1 state. In this case, it is expected that the S_1 state after $S_n \rightarrow S_1$ relaxation is vibrationally excited, because the S_n-S_1 excitation energy ($\sim$17000 cm^{-1}) is initially localized in the generated S_1 molecule. It has been reported that a vibrationally hot S_1 *trans*-stilbene generated by a short-wavelength (226 nm) excitation exhibits broader transient absorption, compared to the spectrum of the thermalized S_1 state.[49] Therefore, the vibrationally hot S_1 state after $S_n \rightarrow S_1$ relaxation should also represents broader S_1 absorption, which is assigned to the origin of the TG1 component. The vibrationally hot S_1 state disappears with the vibrational cooling time of S_1 *trans*-stilbene. The vibrational cooling time of S_1 *trans*-stilbene was reported as 8 ps[50] and 10 $\pm$ 2 ps[51] in ethanol, which is consistent with the temporal behavior of TG1. Figure 10 sketches the relaxation process following the $S_n \leftarrow S_1$ excitation, which gives rise to the slowly decaying traditional TG signals that were observed in the TR-ISRS measurement.

4. Summary

We performed TR-ISRS measurements for an excited-state polyatomic molecule for the first time, taking *trans*-stilbene as the sample. Raman-active vibrations of the S_1 state were successfully observed in the time-domain. The strongest Raman vibration appeared as an underdamped oscillation with a period of 0.12 ps and it lasted up to $\sim$1 ps. The Fourier transform of the oscillatory ISRS component was compared to the available frequency-domain Raman data (> 200 cm^{-1}), and they showed a very good agreement. Although no new Raman-active S_1 vibration was found in the wavenumber region below 200 cm^{-1},

the present TR-ISRS measurement provided spectral information down to 0 cm^{-1}. It was shown that the TR-ISRS method is certainly capable of observing very low-frequency (terahertz) motions of excited-states, which cannot be accessed by ordinary time-resolved frequency-domain Raman spectroscopy.

Traditional TG signals were also observed in the measurements. The origins of the two slowly decaying TG signals were explained as follows: The first two probe pulses (P_1 and P_2) in TR-ISRS measurements excite some amount of S_1 *trans*-stilbene to the S_n state. A portion of the created S_n state is relaxed very rapidly to generate the vibrationally hot S_1 state. It gives rise to a TG signal (TG1) that decays with a time constant corresponding to the S_1 vibrational cooling time. The rest of the photoexcited S_n state does not return to the S_1 state but is relaxed via different pathways. This results in a net loss of the S_1 population, and generates the "bleaching grating". It is the origin of the TG signal (TG2) that slowly decays with a time constant corresponding to the lifetime of S_1 *trans*-stilbene. Owing to the existence of these traditional TG signals, the ISRS signal of S_1 *trans*-stilbene was practically heterodyned.

In this work, we demonstrated a high potential of the time-resolved time-domain Raman spectroscopy. We examined a particular case, *trans*-stilbene, but it is expected that similar signals having same physical origins are observed in this type of measurements in general. We are now applying the TR-ISRS method to the study of excited-state polyatomic molecules for which no vibrational data are available.

Acknowledgment. This work was supported by a Grant-in-Aid for Scientific Research (B) (No. 13440183) from Japan Society for Promotion of Science (JSPS).

References and Notes

(1) Hamaguchi, H.; Gustafson, T. L. *Annu. Rev. Phys. Chem.* **1994**, *45*, 593.
(2) Tahara, T.; Hamaguchi, H.; Tasumi, M. *J. Phys. Chem.* **1987**, *91*, 5875.
(3) Tahara, T.; Hamaguchi, H.; Tasumi, M. *Chem. Phys. Lett.* **1988**, *152*, 135.
(4) Tahara, T.; Hamaguchi, H.; Tasumi, M. *J. Phys. Chem.* **1990**, *94*, 170.
(5) Tahara, T.; Hamaguchi, H. *J. Phys. Chem.* **1992**, *96*, 8252.
(6) Tahara, T.; Hamaguchi, H. *Chem. Phys. Lett.* **1994**, *217*, 369.
(7) Fujino, T.; Tahara, T. *J. Phys. Chem. A* **2000**, *104*, 4203.
(8) Shimojima, A.; Tahara, T. *J. Phys. Chem. B* **2000**, *104*, 9288.
(9) Mizuno, M.; Tahara, T. *J. Phys. Chem. A* **2001**, *105*, 8823.
(10) Silvestri, S. D.; Fujimoto, J. G.; Ippen, E. P.; Gamble, E. B., Jr.; Williams, L. R.; Nelson, K. A. *Chem. Phys. Lett.* **1985**, *116*, 146.
(11) Ruhman, S.; Williams, L. R.; Joly, A. G.; Kohler, B.; Nelson, K. A. *J. Phys. Chem.* **1987**, *91*, 2237.
(12) Ruhman, S.; Joly, A. G.; Nelson, K. A. *J. Chem. Phys.* **1987**, *86*, 6563.
(13) Etchepare, J.; Grillon, G.; Chambaret, J. P.; Hamoniaux, G.; Orszag, A. *Opt. Commun.* **1987**, *63*, 329.
(14) Vöhringer, P.; Scherer, N. F. *J. Phys. Chem.* **1995**, *99*, 2684.
(15) Matsuo, S.; Tahara, T. *Chem. Phys. Lett.* **1997**, *264*, 636.
(16) Joo, T.; Albrecht, A. C. *Chem. Phys.* **1993**, *173*, 17.
(17) Ippen, E. P.; Shank, C. V. *Appl. Phys. Lett.* **1975**, *26*, 92.
(18) Green, B. I.; Farrow, R. C. *J. Chem. Phys.* **1982**, *77*, 4779.
(19) Kalpouzos, C.; Lotshaw, W. T.; McMorrow, D.; Kenney-Wallace, G. A. *J. Phys. Chem.* **1987**, *91*, 2028.
(20) McMorrow, D.; Lotshaw, W. T.; Kenney-Wallace, G. A. *IEEE J. Quantum Electron.* **1988**, *24*, 443.
(21) Cho, M.; Du, M.; Scherer, N. F.; Fleming, G. R.; Mukamel, S. *J. Chem. Phys.* **1993**, *99*, 2410.
(22) Ziegler, L. D.; Fan, R.; Desrosiers, A. E.; Scherer, N. F. *J. Chem. Phys.* **1993**, *100*, 1823.
(23) Castner, E. W., Jr.; Chang, Y. J.; Chu, Y. C.; Walrafen, G. E. *J. Chem. Phys.* **1995**, *102*, 653.
(24) Kinoshita, S.; Kai, Y.; Yamaguchi, M.; Yagi, T. *Chem. Phys. Lett.* **1995**, *236*, 259.
(25) Banin, U.; Ruhman, S. *J. Chem. Phys.* **1993**, *99*, 9318.
(26) Banin, U.; Kosloff, R.; Ruhman, S. *Chem. Phys.* **1994**, *183*, 289.
(27) Emde, M. F.; Baltuška, A.; Kummrow, A.; Pshenichnikov, M. S.; Wiersma, D. A. *Phys. Rev. Lett.* **1998**, *80*, 4645.
(28) Baltuška, A.; Emde, M. F.; Pshenichnikov, M. S.; Wiersma, D. A. *J. Phys. Chem. A* **1999**, *103*, 10065.
(29) Jeoung, S. C.; Takeuchi, S.; Tahara, T.; Kim, D. *Chem. Phys. Lett.* **1999**, *309*, 369.
(30) Green, B. I.; Hochstrasser, R. M.; Weisman, R. B. *Chem. Phys. Lett.* **1979**, *62*, 427.
(31) Courtney, S. H.; Kim, S. K.; Canonica, S.; Fleming, G. R. *J. Chem. Soc., Faraday Trans. 2* **1986**, *82*, 2065.
(32) Oberlé, J.; Aabraham, E.; Ivanov, A.; Jonusauskas, G.; Rullière, C. *J. Phys. Chem.* **1996**, *100*, 10179.
(33) Kamisuki, H.; Moriyama, I.; Igarashi, R.; Adachi, Y.; Maeda, S. *J. Chem. Phys.* **1980**, *73*, 3500.
(34) Payne, S. A.; Hochstrasser, R. M. *J. Phys. Chem.* **1986**, *90*, 2068.
(35) Tahara, T.; Toleutaev, B. N.; Hamaguchi, H. *J. Chem. Phys.* **1994**, *100*, 786.
(36) Takeuchi, S.; Tahara, T. *J. Phys. Chem. A* **1997**, *101*, 3052.
(37) Sarker, N.; Takeuchi, S.; Tahara, T. *J. Phys. Chem. A* **1999**, *103*, 4808.
(38) Fujino, T.; Arzhantsev, S. Y.; Tahara, T. *J. Phys. Chem. A* **2001**, *105*, 8123.
(39) Nelson, K. A.; Casalegno, R.; Miller, R. J. D.; Fayer, M. D. *J. Chem. Phys.* **1982**, *77*, 1144.
(40) Terazima, M. *Chem. Phys. Lett.* **1999**, *304*, 343.
(41) Goodno, G. D.; Astinov, V.; Miller, R. J. D. *J. Phys. Chem. A* **1999**, *103*, 10630.
(42) We used the following functional form as the fitting function for the ultrafast and TG components in the 0.26−2 ps region: $I_{TG}(t_d) = [\Delta n(t_d)]^2 + [\Delta\kappa(t_d)]^2$, $\Delta n(t_d) = \alpha_1 \exp(-t_d/\tau_{ultrafast}) + \alpha_2 \exp(-t_d/\tau_{TG1}) + \alpha_3 \exp(-t_d/\tau_{TG2})$, $\Delta\kappa(t_d) = \beta_1 \exp(-t_d/\tau_{ultrafast}) + \beta_2 \exp(-t_d/\tau_{TG1}) + \beta_3 \exp(-t_d/\tau_{TG2})$, where $\Delta n(t_d)$ and $\Delta\kappa(t_d)$ represent refractive index and absorbance changes, respectively, and α_i and β_i ($i = 1-3$) are preexponential factors. The three exponential terms in $\Delta n(t_d)$ and $\Delta\kappa(t_d)$ correspond to the ultrafast, TG1, and TG2 components. We took account of the instrumental response having the fwhm of 66 fs. The fitting was performed under the condition that only β_2 is negative, as inferred from the temporal behavior of the $\Delta\kappa(t_d)$ observed in the three-pulse absorption measurements. The best-fitted function could reproduce the ultrafast and TG components very well, although the obtained time constants were slightly different from the lifetimes of the three components because the fitting was done for a small time window of 0.26−2 ps.
(43) We used the data up to the t_d time delay of 2 ps because the oscillatory component is clearly observed in this time region. To improve the apparent resolution in the frequency-domain, we added zero data points from 2 to 20 ps in the time-domain before Fourier transformation.
(44) In the case of the heterodyne detection, the effective sensitivity in the frequency space is determined by the intensity autocorrelation of the probe pulse. The width of the intensity autocorrelation (τ_{auto}) can be estimated from that of the instrumental response ($\tau_{inst} = 66$ fs) that is the intensity cross-correlation of the probe pulse and the squared probe pulse. Assuming a Gaussian pulse shape, the width τ_{auto} was calculated as $\tau_{auto} = (4/3)^{0.5} \times \tau_{inst} = 76$ fs. Thus, the effective sensitivity was given by the Fourier transform of the autocorrelation function having the fwhm of 76 fs.
(45) Gustafson, T. L.; Robert, D. M.; Chernoff, D. A. *J. Chem. Phys.* **1984**, *81*, 3438.
(46) Urano, T.; Hamaguchi, H.; Tasumi, M.; Yamanouchi, K.; Tsuchiya, S.; Gustafson, T. L. *J. Chem. Phys.* **1989**, *91*, 3884.
(47) Oberlé, J.; Jonusauskas, G.; Aabraham, E.; Rullière, C. *Opt. Commun.* **1996**, *124*, 616.
(48) Hamaguchi, H. *Chem. Phys. Lett.* **1986**, *126*, 185.
(49) Kovalenko, S. A.; Schanz, R.; Henning, H.; Ernsting, N. P. *J. Chem. Phys.* **2001**, *115*, 3256.
(50) Iwata, K.; Hamaguchi, H. *J. Phys. Chem. A* **1997**, *101*, 632.
(51) Quian, J.; Schultz, S. L.; Bradburn, G. R.; Jean, J. M. *J. Phys. Chem.* **1993**, *97*, 10638.